CHEMISTRY OF MATERIALS
Cite This: Chem. Mater. 2018, 30, 225−238
Article
pubs.acs.org/cm

Characterization of the Ligand Capping of Hydrophobic CdSe−ZnS Quantum Dots Using NMR Spectroscopy

Birong Zeng,[†,‡] Goutam Palui,[†] Chengqi Zhang,[†] Naiqian Zhan,[†,§] Wentao Wang,[†,∥] Xin Ji,[†,∥] Banghao Chen,[†] and Hedi Mattoussi*[,†]

[†]Department of Chemistry and Biochemistry, Florida State University, Tallahassee, Florida 32306, United States
[‡]Department of Materials Science and Engineering, Fujian Provincial Key Laboratory of Fire Retardant Materials, Xiamen University, Xiamen, Fujian 361005, China

Supporting Information

ABSTRACT: We have combined a few advanced solution phase NMR spectroscopy techniques, namely, ^{1}H, ^{31}P, heteronuclear single quantum coherence (HSQC), and diffusion ordered spectroscopy (DOSY), to probe the composition of the organic capping layer on colloidal CdSe−ZnS core−shell quantum dots grown via the "hot injection" route. Combining solution phase ^{31}P and ^{1}H NMR with DOSY, we are able to distinguish between free ligands and those coordinated on the QD surfaces. Furthermore, when those NMR measurements are complemented with matrix-assisted laser desorption ionization (MALDI) and FTIR data, we find that the organic shell of the as-prepared QDs consists of a mixture of tri-*n*-octylphosphine oxide (TOPO), tri-*n*-octylphosphine (TOP), alkyl amine, and alkyl phosphonic acid (L- and X-type ligands); the latter molecules are usually added during growth at a rather small concentration to improve the quality of the prepared nanocrystals. However, NMR data collected from QD dispersions subjected to two or three rounds of purification reveal that the organic shell composition (of purified QDs) is essentially dominated by monomeric or oligomeric *n*-hexylphosphonic acid, along with small fractions of surface-coordinated or hydrogen-bonded 1-hexadecyl amine and TOP/TOPO. This is true even though large excesses of TOP and TOPO surfactants are used during QD growth. This proves that *n*-hexylphosphonic acid (HPA) exhibits substantially higher coordinating affinity to the QD surfaces, compared to other phosphorus-containing surfactants such as TOP and TOPO. Finally, we test the utilitys of DOSY NMR to provide accurate data on the translational diffusion coefficient (and hydrodynamic radius) of QDs, as well as freely diffusing ligands in a sample. This proves that DOSY is a highly effective characterization technique for such small colloids and organic surfactants where DLS reaches its limit.

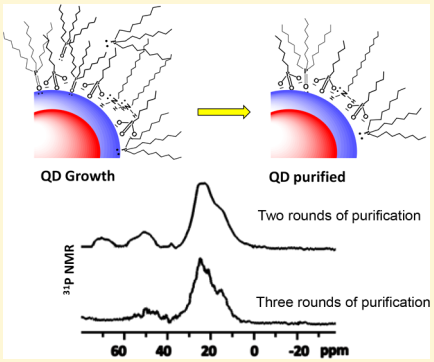

1. INTRODUCTION

Colloidal semiconductor nanocrystals (quantum dots, QDs) are among the most extensively studied nanomaterials, because they exhibit unique size- and shape-dependent optical and spectroscopic properties.[1−7] Core−shell QDs, such as those made of ZnS-overcoated CdSe, show high quantum yield combined with a remarkable photo and chemical stability. These materials have generated great interest and much activity in the past two decades. Several potential applications such as integration in various optoelectronic devices, sensing, and use in fluorescent imaging of cells and tissue have been outlined in recent years.[2,3,8−13] Many of those applications require fine control over the photophysical properties of the nanocrystals (e.g., quantum yield, emission spectra, and colloidal stability). Those properties are directly affected by the presence of surface defects, resulting from incomplete passivation of interfacial atoms by the organic ligands surrounding the nanocrystals. This organic layer plays a role in controlling the growth kinetics but more importantly promotes the colloidal stability of the prepared nanocrystals.[14−18] In recent years, several investigations have focused on developing new and improved growth strategies to obtain better quality QDs, with small size dispersity and high PL quantum yield.[1,19−22] However, interactions of the ligands with the nanocrystals remain difficult to control, and there are few effective methods to identify and quantify the ligand density on the nanocrystals. Indeed, a molecular-scale understanding of the interface between the inorganic cores and ligand shells is challenging. Recently, Rosenthal and co-workers investigated the role of phosphonic acid ligands in controlling the emission from surface states in ultrasmall CdSe nanocrystals.[23] The authors were able to tune the photoluminescence quantum yield (PL QY) as well as the band edge absorption wavelength by varying the chain length of alkyl phosphonic acid. Several other studies have shown that the nature of the ligands and their distribution on the nanocrystal surfaces are important for interpreting the structural and the electronic properties of the colloids.[15,24−30]

Received: October 5, 2017
Revised: November 13, 2017
Published: November 13, 2017

DOI: 10.1021/acs.chemmater.7b04204
Chem. Mater. 2018, 30, 225−238

The investigation of the interface is hampered by the difficulty to discriminate between the atoms at the surface and those within the core of the QDs. In previous studies, understanding and controlling the role of the capping molecules on the electronic properties of a nanocrystal, through ligand engineering, have been demonstrated by indirect means. For instance, changes (increases) in the electric conductivity of nanocrystal films after substituting the native surface cap with short-chain ligands have been reported.[31] Similarly, X-ray photoelectron spectroscopy (XPS) has been employed to probe the oxidation states of surface atoms depending on the nature of the capping molecules.[32,33] Among the various techniques used thus far to characterize the surface capping of these nanocrystals, NMR spectroscopy has become one of the most versatile and effective techniques available to researchers.[34−46] It can provide valuable chemical and structural information and a better understanding of the interactions between the inorganic core and the organic surfactant molecules used to grow colloidal nanoparticles.

Recently, several groups have pioneered the use of solution NMR spectroscopy to investigate the nature of the ligands bound onto CdSe nanocrystals.[40,43,46−53] They showed that among others the organic shell of CdSe (core-only) QDs grown in the presence of organophosphorus ligands is predominantly constituted of either alkylphosphonic acid (such as octylphosphonic acid, OPA), or higher-order condensation products (X-type ligands). For example, Weiss and co-workers prepared CdSe QDs following the route reported by Peng and co-workers,[54] and then combined the use of X-ray photoelectron spectroscopy (XPS) and inductively coupled plasma−atomic emission spectroscopy with solution NMR to investigate the nature of the capping molecules of purified QDs.[43] They reported that ∼84% of the surface was covered by phosphorus impurities, namely, *n*-octylphosphonic acid (OPA) and *P*′-*P*′-(di-*n*-octyl)dihydrogenpyrophosphonic acid (PPA) as stable surface-bound ligands. Groups have probed the structures of various semiconductor nanocrystal materials. However, most of those investigations have centered on ligand characterization of core-only QDs.[43,49,52,53] A few reports detailing the use of NMR techniques to characterize the surface chemistry of core−shell QDs such as InP−ZnS have been published, nonetheless.[38,42,55] Expanding upon those investigations to core−shell QDs, which are being widely used by various research groups for potential applications, will be greatly useful to further advance our understanding of such materials prior to and after overcoating with ZnS or ZnSe shells, for example.

In this study, we combine several solution NMR measurements, including ^{1}H, ^{31}P, heteronuclear single quantum coherence (HSQC), and diffusion ordered spectroscopy (DOSY), with matrix-assisted laser desorption ionization (MALDI) mass spectroscopy to address the following questions: (1) What is the nature of the bound ligands? (2) What is the selective binding affinity of the capping ligands? (3) What is the density of the surface ligands and its dependence on the ligand properties? (4) What is the hydrodynamic radius of CdSe−ZnS nanocrystals in organic solvents? For these purposes, we start by growing core-only QDs using a "hot injection" route, where the pyrolysis of the organometallic precursors is carried out in the presence of tri-*n*-octylphosphine oxide (TOPO) and tri-*n*-octylphosphine (TOP) mixed with 1-hexadecylamine (HDA) and *n*-hexylphosphonic acid (HPA) as coordinating solvent mixture. Then, we overcoat the core materials with ZnS shells.[33,56] The QDs are purified from excess free ligands by applying multiple rounds of precipitation using hexane/ethanol mixtures.[56] Our findings indicate that the surface cap of the as-grown QDs is in fact made of a mixture of X-type ligands (e.g., HPA and its oligomeric version) and L-type ligands (namely, TOPO, TOP, and HDA). However, applying 3 and 4 rounds of purification leaves mainly phosphonate-bound ligands. The ligand composition strongly depends on the growth method used and the number of purification rounds applied. We also extract reliable information on the hydrodynamic radius of two distinct core−shell QDs (one emitting at 540 nm and the other at 570 nm) using data on the translational diffusion coefficient extracted from DOSY (diffusion ordered spectroscopy) experiments. These DOSY data are compared to those collected using dynamic light scattering measurements, and good agreement is found. Additionally, we find that DOSY can yield reliable information on the diffusion coefficient for even smaller objects where DLS encounters severe limitations.

2. EXPERIMENTAL SECTION

2.1. Materials. Selenium pellet (≥99.99%), 1-hexadecylamine (HDA, 90%), 1,2-hexadecanediol (HDDO, 90%), sulfur powder, dibromomethane (99%), and organic solvents (chloroform, methanol, toluene, hexane, etc.) were purchased from Sigma Chemicals (St. Louis, MO). Cadmium acetylacetonate ($Cd(acac)_2$, 98%), zinc acetylacetonate ($Zn(acac)_2$, 98%), tri-*n*-octylphosphine (TOP, 90% and 97%), tri-*n*-octylphosphineoxide (TOPO, 98%), *n*-hexylphosphonic acid (HPA), and hexamethyldisilathiane ($(TMS)_2S$, 98%) were purchased from Alfa-Aesar (Ward Hill, MA). Technical grade tri-*n*-octylphosphineoxide (TOPO, 90%) and diethylzinc (99.9998%) were purchased from Stream Chemicals, Inc. (Newburyport, MA). Deuterated solvents for NMR experiments (e.g., $CDCl_3$ and toluene-d_8) were purchased from Cambridge Isotope Laboratories, Inc. (Andover, MA) and used as received. Moisture- and air-sensitive materials were handled in an MBraun Labmaster 130 glovebox (Stratham, NH). Some of the phosphorus compounds and organometallic precursors used in this study must be handled with great care. For instance, diethyl zinc is pyrophoric while $(TMS)_2S$ has a strong smell. They must be stored and handled under inert conditions. Similarly, $Cd(acac)_2$, TOP, and HPA are irritant and potentially toxic.

2.2. Growth and Characterization of the Quantum Dots. The CdSe−ZnS core−shell QDs used in this study were grown in a two-step process.[33,56,57] In the first step, nearly monodispersed CdSe nanocrystals were prepared by reducing organometallic precursors made of $Cd(acac)_2$ and trioctylphosphine-selenium (TOP:Se) at high temperature (350−360 °C) in a hot coordinating solvent mixture made of TOP, TOPO, HDA, HPA, and HDDO, as described in ref 56. Overcoating the core with a rather thick ZnS shell (5−6 monolayers) in a second step was carried out at a slightly lower temperature (150−180 °C) than that used in the first step.[56] In a typical growth reaction, TOPO (3.2 g), HDA (2.8 g), HPA (0.4 g), and TOP (97%, 2 mL) were mixed in a 100 mL three-neck round-bottom flask fitted with a thermocouple temperature sensor, a condenser, and a nitrogen/vacuum inlet adapter. The content was heated under vacuum to ∼160−180 °C for ∼2 h. Separately, in a scintillation glass vial, a mixture of $Cd(acac)_2$ (0.35 g), HDDO (0.3 g), and TOP (90%, 3 mL) was heated at ∼100 °C under vacuum until the solution became homogeneous. The content was cooled down to 60−70 °C followed by the addition of 2 mL of 1.5 M stock solution of TOP:Se to the mixture; this stock solution was prepared by dissolving 5.92 g of selenium in 50.0 mL of 90% TOP, and was left stirring for 24 h in a glovebox. The atmosphere in the 3-neck flask was switched to nitrogen, and the content was heated to ∼350 °C. The mixture containing the cadmium and selenium precursors was rapidly injected into the flask, and then the temperature was immediately reduced to 90 °C; an absorption spectrum was collected to assess the quality of

DOI: 10.1021/acs.chemmater.7b04204
Chem. Mater. 2018, 30, 225−238

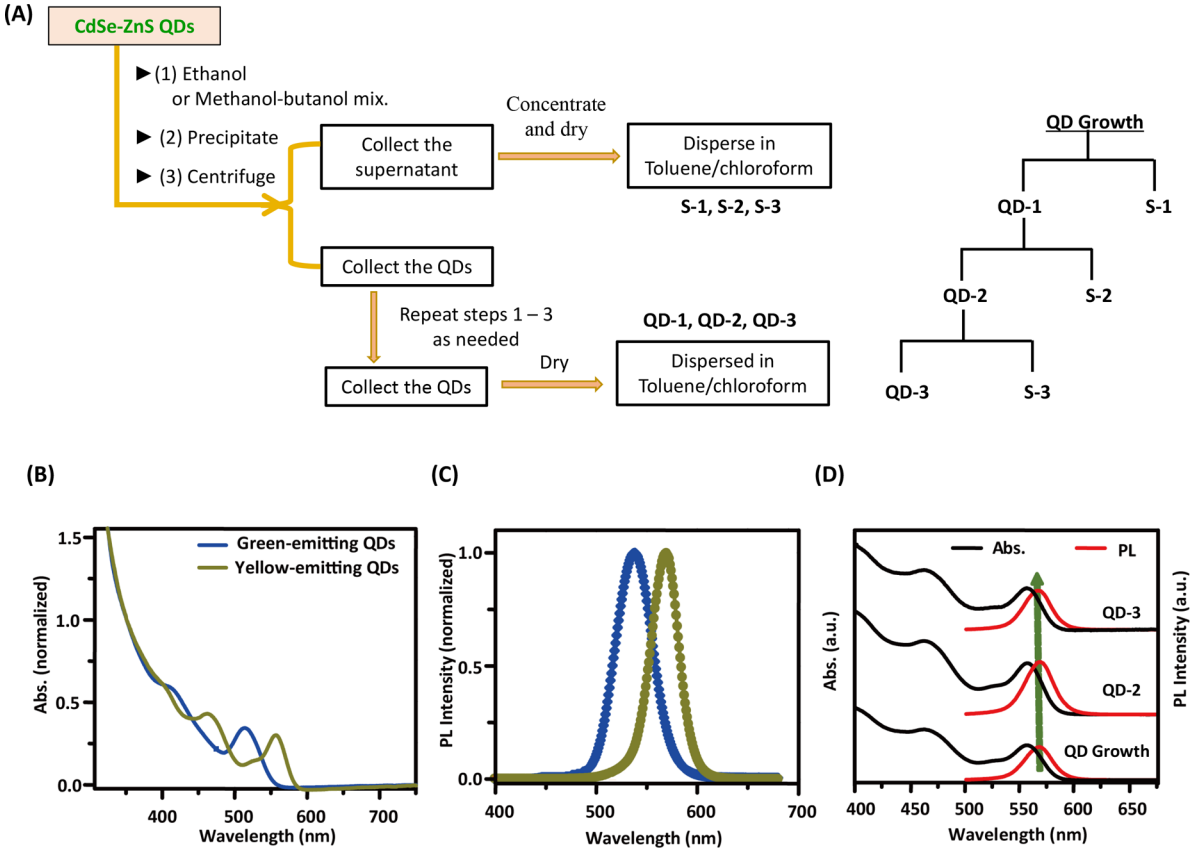

Figure 1. (A) Schematic representation of the purification procedure applied to the growth QDs. After each centrifugation, the pellet is dried under vacuum, then finally dispersed in deuterated solvent to record the NMR spectra. (B) Absorption spectra and (C) emission spectra of green-emitting (λ_{em} = 540 nm) and yellow-emitting (λ_{em} = 570 nm) QDs. The absorption and emission spectra are normalized with respect to the value at 350 nm and emission peak wavelength, respectively. (D) Combined absorption and PL data collected from yellow dots after 2 and 3 rounds of purification then dispersed in toluene. In panels (B) and (C), the absorbance was normalized with respect to the value at 350 nm while the PL was normalized with respect to the peak value.

the initially formed small nanocrystal cores. The temperature was then progressively ramped up to 280−300 °C to allow further growth of the nanocrystals, while monitoring the absorption data. Once the desired absorption spectrum has been identified, growth was stopped by reducing the temperature to ∼70 °C. One round of purification was applied, and the resulting core materials were then used for overcoating with a few monolayers of ZnS. The ZnS-overcoating step was performed using diethylzinc ($ZnEt_2$) and hexamethyldisilathiane ($(TMS)_2S$) as the precursors for zinc and sulfur, respectively.[33,56] The precursors were mixed in 3−5 mL of pure TOP (90%), then added dropwise to a dispersion of CdSe cores in TOPO (to a final Cd concentration of 0.1−0.5 mM). We opted for this route to limit the amount of new ligands introduced. For this we added 6 equiv of the precursors to overcoat the core material following the protocol described in ref 56. The as-prepared core−shell QDs are capped with a hydrophobic organic shell, and therefore are soluble only in organic solvents such as hexane or toluene. They are usually stored in the presence of excess surface cap at room temperature in a mixture of hexane, butanol and toluene until further use. The chemical structure of the precursors, surfactants, and ligands used are provided in the Supporting Information (see Figure S1).

Estimate of the nanocrystal size (i.e., radius) was extracted from TEM data and X-ray scattering.[33,58] The QD concentration was determined from the absorbance spectrum of the dispersion and the extinction coefficient at 350 nm associated with that particular core size, following the procedure developed by Bawendi and co-workers.[59]

2.3. Protocol for the Purification of QDs. The as-grown nanocrystals were purified from excess unbound ligands by applying a few rounds of precipitation and redispersion using hexane/butanol/methanol or hexane/ethanol mixture. Given the importance of the purification to our NMR characterization experiments, we briefly detail the protocol employed to prepare our samples. Here, we have mainly characterized quantum dot dispersions purified once, twice, and three times under ambient conditions. To prepare samples subjected to one round of purification (QD-1), we precipitated 1.5 mL of stock dispersion of hydrophobic QDs (concentration ∼5−15 μM) using 20 mL of ethanol, then centrifugation at 3700 rpm for ∼15−20 min, yielding a paste at the bottom with a clear solution as the supernatant on top. The supernatant was removed which should remove a large amount of unbound ligands from the sample. To prepare dispersions subjected to two rounds of purification (QD-2), we redispersed the paste retrieved from round 1 in hexane (or a mixture of hexane and chloroform), and another round of precipitation using the same volume of ethanol followed by centrifugation was carried out. Dispersion QD-3 was prepared by subjecting the dispersion QD-2 to a third round of purification using the same steps as above. Along with QD-1, QD-2, and QD-3, we will refer to the supernatant solutions collected after one, two, or three rounds of purification as S-1, S-2, and S-3, respectively (see details in Figure 1A). The nanocrystal pellets obtained after each precipitation step were dried under vacuum for ∼120 min, and then redispersed in 550 μL of $CDCl_3$ or toluene-d_8. Conversely, the supernatants were first concentrated using rotary evaporator, dried under vacuum, then dissolved in the desired deuterated solvent. Dispersions of QD-1, QD-2 and QD-3 and solutions of S-1, S-2 and S-3 in deuterated solvents were characterized using the various NMR spectroscopy techniques introduced above.

We would like to note that a fourth round of purification was carried for certain QDs. However, we found that the resulting QD dispersions (QD-4) tend to exhibit limited colloidal stability in certain cases, presumably due to excess ligand removal. Nonetheless, we found

DOI: 10.1021/acs.chemmater.7b04204
Chem. Mater. 2018, 30, 225−238

it useful to characterize the stoichiometry of the resulting supernatant (S-4), in particular when applying mass spectrometry.

2.4. Synthesis of TOP−S and TOPO−Zn Molecular Complexes. *2.4.1. TOPO−Zn.* Several solutions of this complex with varying TOPO-to-Zn molar ratios ranging from 0.25 to 4.0 were prepared by sonicating mixtures of $Zn(acac)_2$, TOPO (∼90%), and deuterated solvent (e.g., $CDCl_3$) for 24 h at 40−50 °C. The solution prepared with the highest molar ratio was slightly turbid, because of the presence of excess insoluble $Zn(acac)_2$ in the sample, indicating a rather limited solubility of the precursor in $CDCl_3$ at higher molar concentrations. All the solutions were centrifuged to remove excess $Zn(acac)_2$ before collecting the ^{31}P NMR data.

2.4.2. TOP−S. A 32 mg (1.0 mmol) portion of sulfur and 0.40 mL of 97% TOP were mixed in a tightly sealed glass vial and left stirring for 24 h under inert conditions (inside the glovebox). The clear supernatant was separated from excess unreacted solid sulfur by applying one round of centrifugation at 3700 rpm for 15 min. Then, 20 μL of the supernatant (TOP:S) was dissolved in 500 μL of dry $CDCl_3$ solution and used to collect the NMR spectra; transfer of the sample to the NMR tube was performed inside the glovebox.

2.5. Instruments. The absorption spectra of the various QD dispersions were recorded using a Shimadzu UV−vis absorption spectrophotometer (UV 2450 model), while a Fluorolog-3 spectrometer (Jobin Yvon Inc., Edison, NJ) equipped with PMT and CCD detectors was used to collect the fluorescence spectra. The solution NMR spectra as well as DOSY spectra were recorded using a Bruker SpectroSpin 600 MHz spectrometer. Dynamic light scattering measurements were carried out using an ALV/CGS-3 compact goniometer system (ALV-GmbH, Langen, Germany). This system is equipped with a HeNe laser (providing illumination at 632.8 nm), a multi-τ photon correlator, and an avalanche photodiode for signal detection. The resulting autocorrelation functions measured at different angles were fitted to a cumulants series using ALV-7004 software to obtain the diffusion coefficients and the hydrodynamic radii of the QDs dispersed in toluene. Mass spectroscopy of the pure organic ligands and those collected from the supernatant solutions, obtained from each washing step, were recorded (in positive mode) using an Autoflex III (matrix-assisted laser desorption ionization, MALDI) instrument equipped with Bruker's patented Smartbeam laser (355 nm, Nd:YAG laser) technology. The TEM images of the QDs were collected using a JEM-ARM200CF instrument (a sub-Angström Cs corrected transmission/scanning electron microscope from JEOL) operated at 200 kV.

2.6. NMR Spectroscopy. All NMR experiments were performed using a Bruker Avance III 600-MHz NMR spectrometer equipped with a 5 mm *z*-gradient Broad Band Observe (BBO) probe operating at 600.13 MHz (for the ^1H frequency), 242.9 MHz (for the ^{31}P frequency) and 150.90 MHz (for the ^{13}C frequency). All measurements were carried out at 293.5 K (∼ room temperature). The following pulse programs were used during data collections:

(a) The ^1H NMR spectra were collected using a pulse repetition time = 25.0 s, a pulse width = 14.0 μs, and acquisition time = 2.0 s. The parameters for collecting the ^{31}P spectra were as follows: pulse repetition time = 1.0 s, pulse width = 14.5 μs, and acquisition time = 0.2 s. The ^{31}P NMR spectra were recorded without proton decoupling, and a line broadening of 50 Hz was applied before Fourier transformation. The ^1H and ^{31}P solution NMR spectra were referenced to tetramethylsilane (TMS) and 85% phosphoric acid, respectively.

(b) The 2D $^{13}C-^1H$ heteronuclear single quantum coherence (HSQC) spectra were acquired using a standard Bruker pulse sequence "hsqcetgpsi.2" with a 90° pulse, a 1.0 s pulse delay, a $^1J_{C-H}$ of 145 Hz, 16 dummy scans, and acquisition of 2048 data points (for ^1H) and 256 increments (for ^{13}C). The central solvent peak was used for chemical shift calibration.

(c) Diffusion ordered spectroscopy (DOSY) data were acquired using the LED-bipolar gradients pulse sequence "ledbpgp2s" with 24k and 32 points in t_2 and t_1, respectively, and each 2D slice represents the signal average of 32 scans. The typical experimental parameters for a DOSY spectrum were as follows: gradient strength = 45 G/cm, diffusion delay time = 300 ms, gradient duration = 1.8 ms, and relaxation delay = 5.0 s. Reference deconvolution and baseline correction were adopted to compensate for the experimental errors.

2.7. Matrix-Assisted Laser Desorption Ionization (MALDI) Spectroscopy. The ligand compounds collected in the supernatants were analyzed by MALDI mass spectroscopy. For preparation of the matrix solution, 10 mg of 3,5-dimethoxy-4-hydroxycinnaminic acid was first dissolved in 700 μL of methanol containing 1% TFA (1% trifluoroacetic acid), and then, 300 μL of 1% TFA and water mixture was added. The solution was sonicated for 15 min, and then centrifuged to remove the insoluble solid matrix material. A 50 μL portion of this matrix solution was mixed with 5 μL of each concentrated supernatant solution collected after each round of purification. The samples were placed on a metal plate as droplets, dried in air, and then analyzed using MALDI-TOF (Bruker Autoflex III) spectrometry.

3. RESULTS AND DISCUSSION

3.1. Rationale for the Characterization Strategy Based on NMR Spectroscopy. Characterizing the structure and nature of the organic surface layer of CdSe−ZnS nanocrystals is crucially important as these materials constitute a sizable fraction of QD materials used in a variety of applications. NMR is a highly suitable technique for achieving this goal. As-grown CdSe−ZnS QDs are typically surrounded by an organic shell which plays a crucial role in maintaining the steric stabilization of the colloidal dispersion while providing electronic passivation of surface states and promoting enhanced radiative recombination of e−h pairs and high PL QY.[60] There is, in principle, a dynamic equilibrium between surface-bound and freely diffusing ligands in the dispersion, which is shifted toward lower concentrations of ligands exhibiting higher coordinating affinity to the inorganic surface of the nanocrystals.[61] This equilibrium can be further affected by introducing excess ligands in the medium. To identify the nature and abundance of the surface-bound versus free ligands in dispersions of core−shell QDs, we characterize the ligand composition on the nanocrystals for all three sets of purified QD dispersions (QD-1, QD-2 and QD-3) simultaneously with the ligand mixtures detected in solutions S-1, S-2, and S-3, using a combination of solution phase ^1H and ^{31}P, HSQC and DOSY NMR, along with mass spectroscopy.

3.2. UV−Vis Absorption and Photoluminescence of the QDs. Figure 1B,C shows the absorption and PL spectra of two sets of core−shell QDs, emitting at 540 nm (green QDs) and at 570 nm (yellow QDs) dispersed in toluene. The well-defined spectra indicate that the QD dispersions are homogeneous and contain low-size-dispersity nanocrystals. The optical features remain unaltered even after a few rounds of purification. Nonetheless, the dispersions become progressively unstable with signs of aggregation build up occurring when four or higher rounds of purification are applied. This may indicate that deficiency in the surface coverage of the nanocrystals, due to a drastic decrease in ligand concentration, starts to alter the steric stability of the QD dispersions.[58]

3.3. Ligand Identification on the QD Surfaces. *3.3.1. ^{31}P NMR Spectroscopy.* The "hot injection" growth route uses several coordinating ligands including large amounts of TOP and TOPO, mixed with smaller concentrations of cosurfactant, metal-coordinating molecules such as HPA and HDA. We first employed ^{31}P NMR to identify the presence of phosphorus-containing compounds. Figure 2A−D shows the

DOI: 10.1021/acs.chemmater.7b04204
Chem. Mater. 2018, 30, 225−238

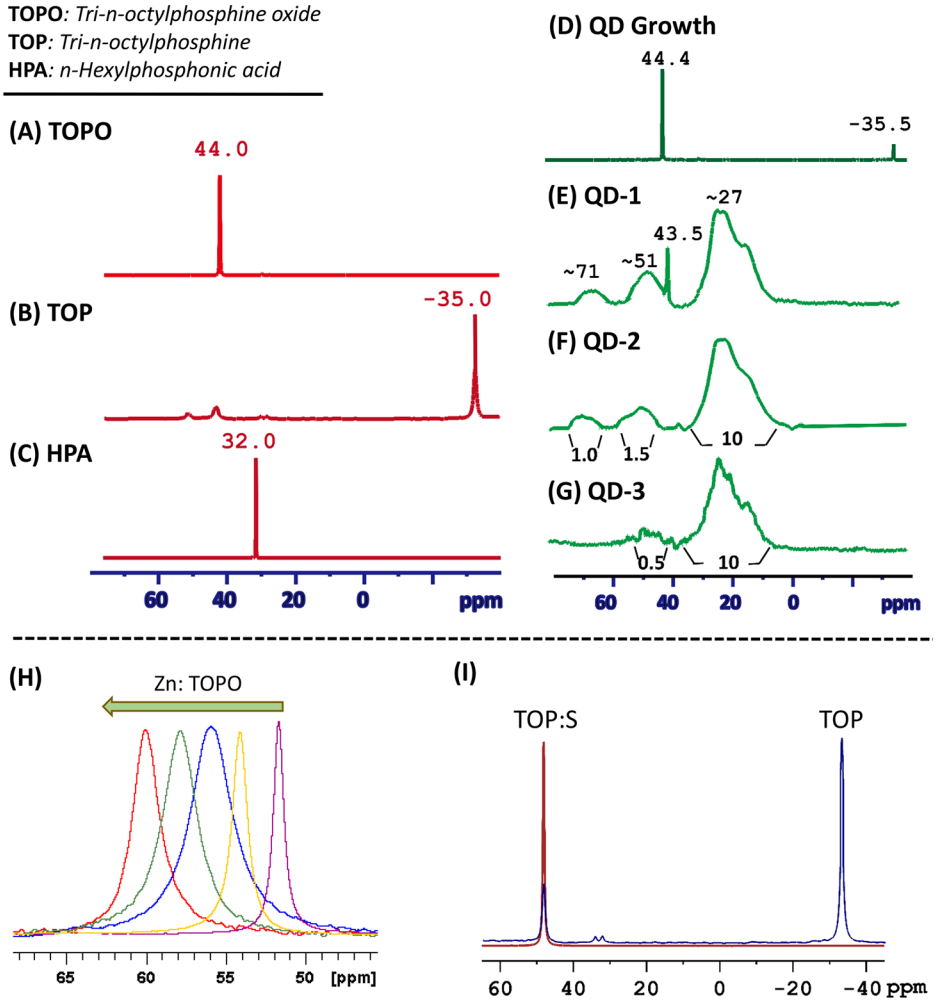

Figure 2. ^{31}P NMR spectra of the following: (A) TOPO, (B) TOP, (C) HPA, (D) growth QDs, (E) QDs after one round of purification (QD-1), (F) QDs after two rounds of purification (QD-2), and (G) QDs after three rounds of purification (QD-3); QDs with emission at 540 nm have been used. Also shown are ^{31}P NMR spectra of (H) mixtures of Zn(acac)$_2$ and TOPO; the shown spectra, from right to left, are for TOPO−Zn molar ratios of 0.25:1, 0.5:1, 1:1, 2:1, and 4:1. (I) Overlap of two NMR spectra of TOP (blue line) and TOP:S (red line).

spectra of TOPO, TOP, and HPA together with the one collected from an aliquot of the growth QDs (emitting at 540 nm) dispersed in toluene-d_8. Clearly the spectra show characteristic peaks with measured chemical shifts at the following: 44.0 ppm (for TOPO), −35.0 ppm (for TOP), and 32.0 ppm (for HPA). The sharp features shown in Figure 2A−C are due to rapid molecular motions of free ligands in solution. Two sharp peaks are also measured at 44.5 and −35.5 ppm for the growth dispersion of QDs (see Figure 2D), implying that large concentrations of TOP and TOPO molecules present in the dispersion are unbound. However, the spectrum collected from the purified dispersion QD-1 shows weaker, broadened signatures, albeit a sharp signature at $\delta \cong 43.5$ ppm is also measured (see Figure 2E); the latter is associated with the presence of a small fraction of free TOPO molecules in the sample. This implies that the majority of the detected ligands in QD-1 are coordinated with the metal-rich surface of the nanocrystals, and they experience substantially slower motions, yielding weaker NMR spectra with broadened features. The spectrum collected from QD-2 shows only broadened features with chemical shifts centered at ∼27, ∼ 51, and ∼71 ppm that are different from those peaks associated with free TOP and TOPO (compare Figure 2F to Figure 2A,B). Similar ^{31}P NMR spectra for the yellow-emitting QDs are shown in the Supporting Information, Figure S2. This indicates the presence of three distinct sets of surface-bound phosphonate ligands. Conversely, the spectrum collected from a dispersion subjected to a third round of purification (QD-3) shows only a clearly defined signal at ∼27 ppm, but a much weaker signature at ∼51 ppm, while the signal at ∼71 ppm has disappeared (Figure 2G). We attribute the stronger peak at ∼27 ppm to phosphonic acid molecules (such as *n*-hexylphosphonic acid, HPA) coordinated onto the ZnS surface of the QDs. Indeed weak features with chemical shifts located at ∼20−40 ppm have been reported and attributed to monomers and oligomers of octylphosphonic acid (OPA) bound to the QDs (e.g., ref 43).

These findings indicate that all the residual weakly bound TOP and TOPO are essentially removed from the sample after two rounds of purification. The remaining two other peaks at ∼51 and ∼71 ppm (shown in Figure 2E−G) can tentatively be ascribed to sulfur-complexed TOP and Zn-complexed TOPO. To confirm this assignment, we collected the ^{31}P NMR spectra of molecular complexes TOPO−Zn and TOP−S, which were, respectively, prepared by mixing TOPO with Zn(acac)$_2$ and TOP with sulfur, as described in the Experimental Section.

DOI: 10.1021/acs.chemmater.7b04204
Chem. Mater. 2018, 30, 225−238

Figure 2H shows the ^{31}P NMR spectra collected from solutions of Zn(acac)$_2$ and TOPO in $CDCl_3$ having a Zn-to-TOPO molar ratio varying between 0.0:1 and 4:1. The peak position of TOPO moves downfield (from δ = 44 to 66 ppm) with increasing amount of added Zn(acac)$_2$ to the solution. This can be ascribed to coordination interaction between TOPO and the Zn, i.e., increasing concentration of Zn complexed with TOPO molecules. Note that only a limited concentration of Zn(acac)$_2$ can be dissolved in $CDCl_3$ (indicating rather modest solubility of the Zn-precursor/complex in the NMR solvent). We thus assign the broad resonance peak centered at ∼71 ppm with a peak width range 63−80 ppm (measured for QD-2) to Zn-coordinated TOPO on the QDs; here the nanocrystals offer a zinc-rich surface for TOPO coordination in the form of TOPO−Zn. Similarly, the data obtained from a solution of TOP−S in $CDCl_3$ show that the chemical shift of this complex is at ∼50 ppm, which is similar to the one at ∼51 ppm (compare spectra in Figure 2I and Figure 2E−G).

To further confirm the persistence of surface-coordinated TOPO on the QDs after 2 rounds of purification (i.e., QD-2), we combine the data shown in Figure 2E−G with the information deduced from the additional ^{31}P NMR spectra collected from the supernatant solutions S-1, S-2, and S-3 (see Figure 3A−C). The ^{31}P NMR spectrum obtained from S-1

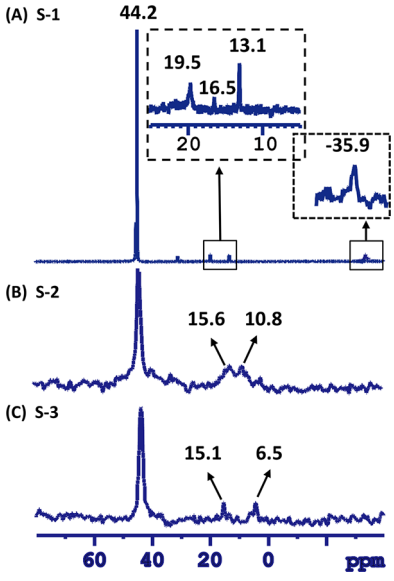

Figure 3. ^{31}P NMR spectra of supernatant solutions retrieved from (A) one round of purification (S-1), (B) two rounds of purification (S-2), and (C) three rounds of purification (S-3). The chemical structures of the higher-order phosphonic acid oligomers or potential condensation products of HPA (deprotonated products) which show chemical shift at ∼10−20 ppm are provided in the Supporting Information (Figure S1).

(Figure 3A) shows two peaks that correspond to the free TOPO (at ∼44.2 ppm) and TOP (at ∼−35.9 ppm), though the latter is substantially weaker, along with four other weak signatures at ∼32.0, ∼19.5, ∼16.5, and ∼13.1 ppm. The spectra collected from the supernatants S-2 and S-3 show a prominent sharp peak at ∼44.2 ppm ascribed to the free TOPO, along with a few very small peaks in the range ∼10−30 ppm. The decrease in the peak intensities at ∼51 and ∼71 ppm measured for QD-2 and QD-3 (Figure 2F,G), combined with the presence of a large peak at ∼44 ppm measured in S-2 and S-3 (Figure 3A−C), confirm that large amounts of TOPO ligands have been removed from the QD dispersion during the first and second rounds of purification, though very small amounts of TOP and TOPO complexed with the zinc- and sulfur-rich surface of the nanocrystals are detected. We also note that the TOP signal (at ∼−35.9 ppm) is weak and detected only for sample S-1 but not in the supernatants S-2 and S-3. We attribute this to the fact that TOP tends to easily oxidize to TOPO, which may explain the comparatively strong peak at ∼44 ppm. Similarly, the small signals at ∼6.5−15.6 ppm measured in the ^{31}P NMR spectra from solutions S-2 and S-3 can be ascribed to displaced higher-order phosphonic acid oligomers or deprotonated HPA during the rounds of purification.[43,51]

The above ^{31}P NMR data combined show that TOPO and TOP molecules coordinate to the nanocrystals, and the bound ligands are easier to observe in the presence of high overall surfactant concentrations (e.g., in growth QDs and QD-1). They can however be more easily detached from the QD surfaces during additional rounds of purification. However, we do not observe any large signal corresponding to HPA in Figure 3B,C, which suggests that most of the phosphonic acid compounds stay attached to the nanocrystal surface after 2 and 3 rounds of purification. Such a result can be attributed to the stronger binding affinity of these molecules to the QDs (i.e., lower dynamic off rates). To gain further insights into the composition of surface-bound molecules, we apply additional NMR spectroscopy measurements discussed below.

It is noted that even though HPA was used only for the core growth reaction, our findings indicate that the alkyl phosphonates are disproportionally represented in the final surface ligand stoichiometry of the purified core−shell QDs (e.g., their number exceed 50% of the total number of ligands). This can be attributed to a combination of two factors: (1) The purification of the native core-only dispersions involves one round of purification, which undoubtedly leaves non-negligible amounts of soluble phosphonates and HDA in the medium during the overcoating step. (2) A strong coordination between the nanocrystal surfaces (CdSe core-only and Core−shell) and phosphonate ligands. The dynamic on/off interactions between the ligands and metal surfaces facilitate the slow growth of the ZnS overcoating, but the higher affinity of those ligands to the surfaces is preserved when the final core−shell nanocrystals are formed.

3.3.2. 1D ^{1}H NMR and 2D (HSQC and DOSY) NMR Spectroscopy. Figure 4A−D shows the ^{1}H NMR spectra of solutions of TOPO, HPA, and HDA together with the spectrum collected from a dispersion of green-emitting QDs subjected to two rounds of purification (QD-2). The resonances ascribed to the methyl and methylene protons in TOPO, HPA, and HDA, which appear in the aliphatic region of the ^{1}H NMR spectrum (0.8−2 ppm range), are sharp and share a strong overlap (see Figure 4A−C). In comparison, the spectrum collected from the QD dispersion (QD-2) shows a few broad resonances, namely, three broad peaks at ∼1.0, ∼1.2−1.8, and ∼3.20 ppm, along with one sharp singlet peak at 1.38 ppm and two triplet peaks at 0.95 and 2.09 ppm (see Figure 4D). We conclude from a close examination of the various spectra shown in Figure 4A−D that alkyl-containing molecules are bound onto the QD surfaces, which broadens some of the proton signatures associated with those ligands. In particular, we ascribe the broad peak at ∼3.20−3.40 ppm to the amine group of QD-bound HDA, as binding of the ligand to

DOI: 10.1021/acs.chemmater.7b04204
Chem. Mater. 2018, 30, 225−238

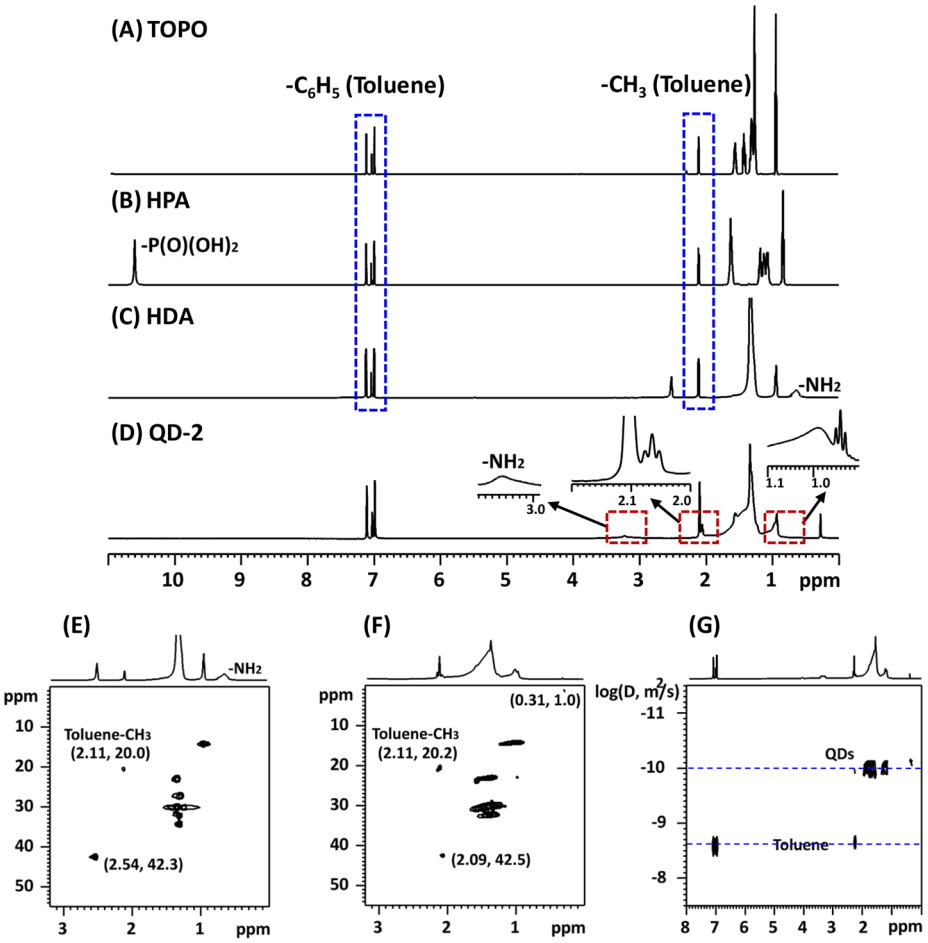

Figure 4. ^{1}H NMR spectra of (A) TOPO, (B) HPA, (C) HDA, and (D) green-emitting QDs subjected to two rounds of purification (QD-2). The peaks at ∼3.2, ∼2.1, and ∼0.9 ppm (shown in panel D) are expanded (×16) using NMR software. HSQC spectra of (E) alkylamine (here HDA) and (F) QD-2, where the ^{13}C chemical shift at ∼42 ppm corresponds to the $-CH_2$ adjacent to the primary amine. (G) DOSY spectra of QD-2 in toluene where only one diffusion coefficient is measured; the signature at ∼2.09 ppm is clearly shown.

the nanocrystal alters the environment of the primary amine active protons, thus shifting its signature toward downfield. However, better characterization of the three peaks (at 0.95, 1.38, and 2.09 ppm) can be established using proton−carbon heteronuclear single quantum correlation (HSQC) spectroscopy. In such an experiment, the shift ascribed to the carbon adjacent to the electronegative heteroatoms is much easier to distinguish, because of the large downfield chemical shift compared to other carbons along the chain. One can thus use the data to correlate the proton resonances with those of carbon atoms in the same molecules. Figure 4E,F shows the HSQC spectrum of HDA side-by-side with that collected from the dispersion QD-2, both in toluene-d_8. It is well-established that the chemical shifts of all carbon atoms in TOPO, TOP, and HPA are lower than 40 ppm.[48] However, the carbon adjacent to the amine group ($-CH_2NH_2$) in HDA has a characteristic chemical shift above 40 ppm, due to the presence of electronegative nitrogen.[62] Figure 4E shows that the proton in the terminal $-NH_2$ group of free HDA located at ∼0.66 ppm has no cross-peak as expected, while the methylene group adjacent to the amine (i.e., $-CH_2NH_2$) presents one cross-peak at (∼2.54 ppm, ∼42.3 ppm). A similar characteristic cross-peak at (∼2.09 ppm, ∼42.5 ppm) is observed in the 2D spectrum obtained from the QD-2 sample (see Figure 4F). We thus tentatively assign this cross-peak to the methylene protons of HDA "bound" to the QD surface. However, identifying the two cross-peaks associated with ^{1}H shift at 1.38 and 0.95 ppm (in Figure 4F) is less obvious, because of the strong overlap in the carbon signatures for all three molecules, TOPO, TOP, and HPA; those signatures are observed in the range from ∼10 to ∼35 ppm (see ^{13}C spectra in the Supporting Information, Figure S3). A close inspection of the proton peaks at 3.20, 2.09, and 0.95 ppm (shown in Figure 4D) indicates that the integration values satisfy a ratio of 2:2:3, as anticipated from the stoichiometry of those groups (NH_2:CH_2:CH_3). We can thus confirm that these three resonance peaks are ascribed to HDA. The latter was used in the growth of the core materials, but not completely removed prior to the overcoating step.[56]

Further insights into the interactions of HDA with the QD surfaces can be gained from correlating the proton resonance at 2.09 ppm with the other two resonances at 1.38 and 0.95 ppm, using diffusion ordered spectroscopy (DOSY). According to its principles this technique probes the Brownian motion of soluble objects, and molecules with different molecular weights (or sizes) exhibit different translational diffusion coefficients. The DOSY spectra of green QD-2 and solubilized toluene are shown in Figure 4G (log(D) versus ^{1}H NMR shift). The spectrum shows only two sets of diffusion coefficients, which are different from the value extracted from the DOSY data for the free unbound ligand (e.g., HDA; see the Supporting

DOI: 10.1021/acs.chemmater.7b04204
Chem. Mater. 2018, 30, 225−238

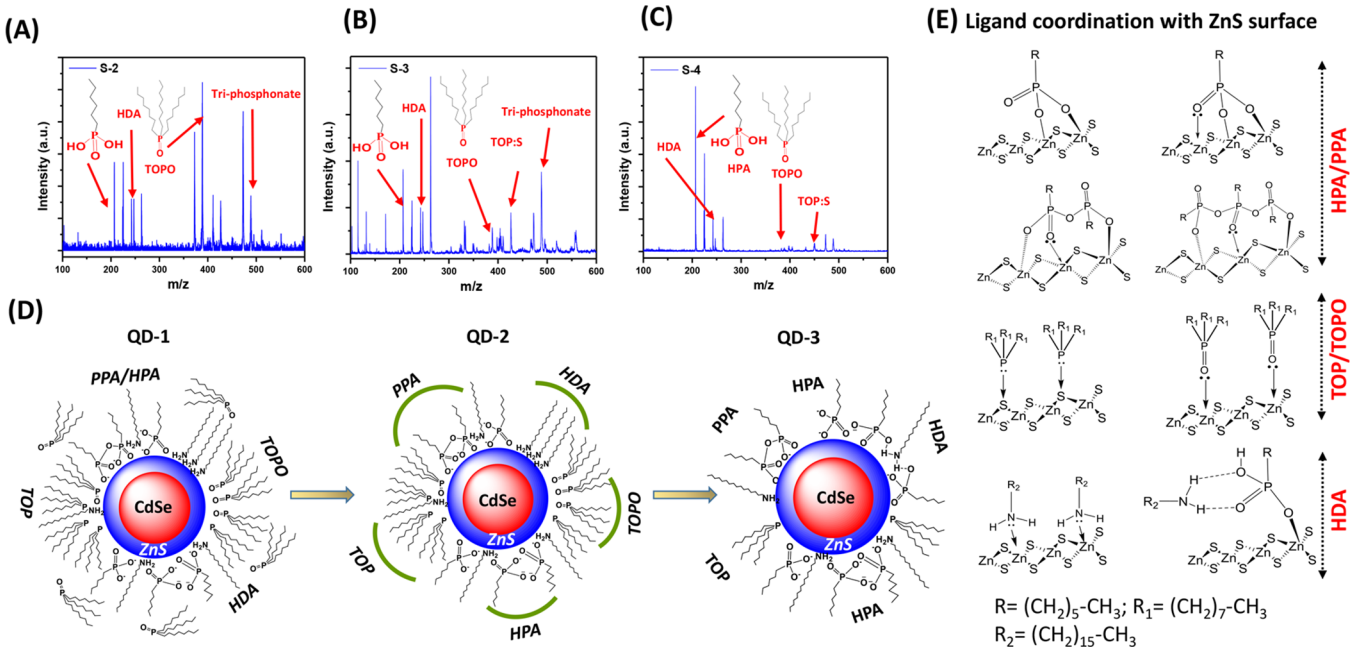

Figure 5. MALDI-MS spectroscopy data collected from the supernatant after (A) two, (B) three, and (C) four rounds of purification (using green-emitting QDs). The recorded peaks in the mass spectra appear either as molecular ions or molecular ion combined with sodium and/or potassium cations. MALDI collected from S-1 contains only unbound ligands, and therefore data are not shown. (D, E) Proposed model of the bound ligands and nature of interactions onto the dot surface. Note that chargeable ligands such as phosphonate and carboxylate types are referred to as X-type while neutral ligands such as TOPO, TOP, and HDA are referred to as L-type following the classification proposed by Green.[72]

Information, Figure S4). One set is associated with toluene molecules ($D_{tol} \sim 2.03 \times 10^{-9}$ m^2/s at 293.5 K) comparable to the value reported by Hens and co-workers $D_{tol} \sim 2.13 \times 10^{-9}$ m^2/s at 295.0 K.[37] The other measured for the three resonance peaks at 2.09, 1.38, and 0.95 ppm (shown in Figure 4D) can be ascribed to QD-bound HDA ligands. The signal of α-CH_2 of bound HDA is rather weak in the DOSY spectrum shown in Figure 4G. This is due to the fact that those protons have a short T2 relaxation time, smaller than the delay required to extract the Brownian diffusion. Their signature will therefore be weakened in the measured spectrum.[52] These findings indicate the absence of any detectable free ligand in the QD dispersion (QD-2). Similar characteristic peaks are observed for the yellow QDs obtained after two rounds of purification (see the Supporting Information, Figure S5).

We should also note that the triplets at ∼0.95 and ∼2.09 ppm and the singlet at ∼1.38 ppm are still well-defined and distinguishable from the broad signals measured in the spectrum collected from QD-2 (Figure 4D). This result can be attributed to two complementary factors: (1) Though direct coordination of amine-terminated ligands to the nanocrystals has been proven, HDA attachment onto the QD surface can additionally occur by tight association between HDA and alkyl hydrogen phosphonate (HPA) via hydrogen bond, as proposed by Hens and co-workers, or via ion pair formation (NH_2R'/$[O_3PR]^-[H_3NR']^+$) as recently suggested by Owen and co-workers.[63] Both modes of interactions bring the ligands in close proximity to the nanocrystal surface.[14,49,63] (2) Because of its longer alkyl chain (compared to HPA or TOPO), surface-associated HDA chains will show faster proton relaxation synonymous to those of free molecules in solution. Association of HDA ligands with the QD surfaces is further supported by additional ^{1}H NMR data collected from the yellow-emitting QD sample subjected to two rounds of purification QD-2, where the proton peaks at 0.95, 2.09, and 3.40 ppm are measured (see the Supporting Information, Figure S5). This further confirms that after applying one additional round of purification a fraction of the surface-bound ligands is made of HDA. Additional proofs are discussed in the section describing the mass spectroscopy data, shown below.

We should note that HDDO which is used in the growth of the cores does not play a role in the ligand shell and is removed during the purification steps. Indeed, we collected ^{13}C NMR spectra from a solution of HDDO in $CDCl_3$ and measured two sets of peaks, one in the range 10−35 ppm associated with the methylene carbon atoms and the other at 65−70 ppm associated with the carbon attached to the electronegative oxygen heteroatom (see the Supporting Information, Figures S1 and S6). We have not measured any of those signatures in the HSQC spectra of the purified QDs shown in Figure 4.

3.3.3. Matrix-Assisted Laser Desorption Spectroscopy. The ^{31}P NMR data obtained from the supernatant solutions S-1, S-2, and S-3 (shown in Figure 3) have been further complemented with mass spectroscopy data. More precisely, mass spectroscopy measurements were carried out to characterize the supernatant solutions S-1, S-2, S-3, and S-4 collected from both sets of QDs; S-4 designates the supernatant collected after four rounds of purification. Figure 5 shows the MALDI-MASS spectra collected from S-2 to S-4 corresponding to green-emitting QDs. Spectra show that there are signatures of TOPO and HDA in S-2 and S-3 (Figure 5A,B). The TOPO signature is, however, substantially smaller in S-4 (Figure 5C). We also observed a small peak in the supernatants S-3 and S-4 (which are obtained from QD-2 and QD-3, respectively), corresponding to TOP−S. This indicates that QD surfaces lose few weakly bound sulfur atoms during the ethanol wash. Additionally, we detect the presence of HPA molecules (monomers and oligomers) in the supernatants S-2, S-3, and

DOI: 10.1021/acs.chemmater.7b04204
Chem. Mater. 2018, 30, 225−238

S-4, which correlates well with the data obtained from the ^{31}P NMR discussed above (Section 3.3.1). The TOP and TOPO ligands bind weakly to the ZnS surface and, therefore, can easily be desorbed from the QDs after two or three rounds of purification using ethanol or methanol. Because of their nature, TOP molecules are rapidly oxidized to TOPO after release from the nanocrystal surface. They thus are not accounted for in the mass spectroscopy data.

We would like to stress that though HPA and derivatives exhibit the strongest coordination interactions with the QD surfaces, long-term colloidal stability requires the presence of TOP, TOPO, and HDA ligands. In fact, QD dispersions subjected to more than four rounds of purification tend to become unstable, as aggregation builds up with time.[56]

On the basis of the NMR data and analysis of the mass spectroscopy data discussed above, we conclude that, in a QD growth dispersion, TOPO, TOP, HPA and HDA are all absorbed on the QD surface, though the coordination affinity may drastically vary from one ligand to another. Phosphonate ligands tend to exhibit the strongest coordination interactions, and they persist through a few rounds of purifications. HDA and TOPO also adsorb, but interactions with the inorganic surface of the QDs are weaker. Though TOP and TOPO interact directly with the ZnS-rich QD surface, binding of HDA potentially involves direct coordination and/or hydrogen bonding with the surface-coordinated phosphonate ligands. Schematics of the suggested model for the ligand composition on the QD surfaces are shown in Figure 5E.[64]

We should note that the conclusions drawn from the NMR data on the composition of the surface-bound ligands for QD dispersions, subjected to three rounds of purification, are further supported by FTIR data collected from pure ligands and QD-3. For example, the binding of HDA is confirmed by the red shift in the stretching and bending frequencies of NH_2 (ν_{N-H} and δ_{N-H}) in the spectra collected from the QD-3 sample. Also, the change in the symmetric and asymmetric stretching of P−OH in the QD sample compared to that associated with the unbound HPA assures strong binding of the ligands onto the nanocrystal surfaces. Additionally, minimal to no change in the frequencies, $\nu(CH_2)$ and $\nu(CH_3)$ ascribed to the alkyl chains in the various ligands, was measured. Further discussion along with the FTIR data are provided in the Supporting Information (see Figure S7 and Table S1).

3.3.4. Quantifying the Ligand Composition. The solution NMR and mass spectroscopy analyses have shown that the mixture of the remaining QD-bound ligands, after two rounds of purification, include TOPO, TOP, HPA and HDA, though the abundance of each compound varies. Data also show that the purification strategy and steps applied play a role in the composition of the remaining organic surface layer. To quantify the ligand composition, we use diboromomethane as a standard for our ^{1}H NMR measurements, because it has a proton resonance (at 4.94 ppm) that does not overlap with those ascribed to the bound ligands. We analyzed the spectra collected from QD-3 dispersions in either toluene-d_8 or $CDCl_3$. We are more confident in the analysis of the data collected from dispersions in $CDCl_3$, where the resonance signatures of the HDA methylene protons at 2.39 ppm and the terminal methyl protons in the alkyl chain(s) of all ligands at 0.89 ppm have no interference from the chloroform solvent; the proton signatures at 0.89 and 2.39 ppm are, respectively, used to quantify the total amount of alkyl chains and the fraction of HDA in the ligand shell. Conversely, in toluene-d_8 the solvent signature slightly overlaps with those protons. (Toluene has a sharp singlet at 2.12 ppm very close to the CH_2−NH_2 of HDA at 2.09 ppm; see Figure 4E−G.) Therefore, we rely on the terminal amine proton signature at 3.2 ppm to extract an estimate for the amount of QD-bound HDA; spectra of QD-3 collected in toluene are provided in the Supporting Information, Figure S8. We should also emphasize the fact that the proton signatures (e.g., the methylene protons of HDA adjacent to the amine or the terminal methyl groups of long-chain alkane), measured in $CDCl_3$, are shifted compared to those measured in toluene-d_8. This is due to differences in the polarity between the two deuterated solvents; the ^{1}H NMR and HSQC spectra of HDA in $CDCl_3$ are provided in the Supporting Information, Figure S9.

A few additional complications related to the structure of the ligands used must also be taken into account. One is due to the fact that in the ^{1}H NMR spectra all CH_3 protons in TOP, TOPO, HPA, and HDA generate a similar shift at 0.89 ppm. The other complication is related to the fact that TOP and TOPO contain three alkyl chains per molecule, while HPA and HDA contain one chain per molecule.

Quantification of the number of ligands per nanocrystal in QD-3 is carried out in a few steps: (1) We first make use of the ^{31}P NMR data (shown in Figure 2 and Figure S2) to quantify the stoichiometry of the phosphine-containing ligands in the organic shell. That composition is TOP:HPA = 1:20 (for green QDs) and 1:6 (for yellow QDs); no TOPO was detected in QD-3. (2) We extract an estimate for the molar concentration of surface-associated HDA by comparing the integrated intensity of the HDA methylene proton peak (at 2.39 ppm) to that of the standard (at 4.94 ppm; shown in Figure 6). (3) From the integrated area of the methyl proton resonance centered at 0.89 ppm, we deduce a measure for the total molar concentration of QD-bound alkyl chains, that is, the combined molar concentration of alkyl chains of TOP, HPA, and HDA

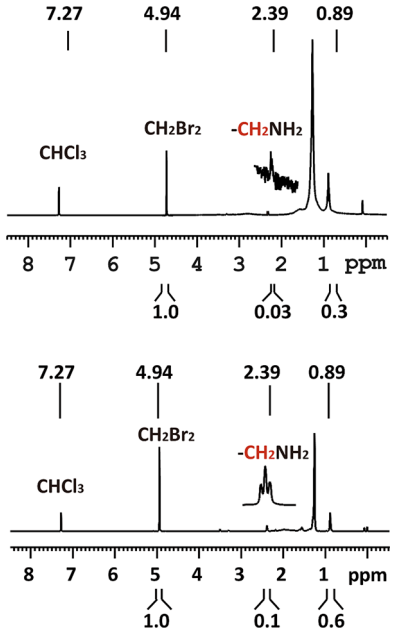

Figure 6. Quantitative analysis of the ligands composition on the QD surfaces: ^{1}H NMR of the green (top) and yellow (bottom) QDs in chloroform-*d* obtained after three rounds of purification. CH_2Br_2 is used as a standard with known concentration.

DOI: 10.1021/acs.chemmater.7b04204
Chem. Mater. 2018, 30, 225−238

Table 1. Ligand Composition for QD-3 (Dispersions Subjected to 3 Rounds of Purification)

QD sample (TEM radius)	concentration (μM)	TOP:HPA ratio	number of TOP groups	number of HPA groups	number of HDA groups	total number of ligands	ligand density[a] (nm^{-2})
green QDs (2.0 nm)	7.0	1:20	9	179	42	230	~4.6
yellow QDs (2.2 nm)	11.5	10:60	34	195	81	310	~5.1

[a]Ligand density = (total number of ligands)/$4\pi R^2$, R = radius of the QD extracted from TEM data.

compared to the molar concentration of the methylene proton of the reference CH_2Br_2. (4) Subtracting the molar amount of HDA (i.e., alkyl of HDA extracted in step 2) from the total concentration of alkyl chains yields a measure of the total concentration of alkyl chains associated with TOP and HPA. (5) We then use the ratio TOP:HPA to estimate the molar fraction of each molecule in the mixture; the TOP fraction is divided by three to account for the presence of 3-alkyl chains in its structure.

Figure 6 shows the ^{1}H NMR spectrum collected from green-emitting QDs dispersed in 500 μL of $CDCl_3$ containing of 14.1 μM CH_2Br_2. The spectrum shows a triplet peak at 2.39 ppm assigned to the methylene group of HDA adjacent to the amine ($-CH_2NH_2$) along with a peak at 0.89 ppm ascribed to the CH_3 groups in the alkyl chains. We first extract the concentration of HDA by calculating the ratio of the areas under the triplet peak at 2.39 ppm and the standard peak at 4.94 ppm (ratio = 1:0.1 for yellow and 1:0.04 for green QDs). We then combine that with the TOP:HPA ratio (1:20 for green and 1:6 for yellow QDs) extracted from ^{31}P NMR (see Figure 4) to obtain the molar concentration of TOP and HPA individually using the integration of the CH_3 resonance at 0.89 ppm. The amount of individual ligands per QD is obtained by comparing the concentration of the added standard to that of the QDs in the sample; the latter is extracted from the UV absorption spectrum using the molar extinction coefficient of the green QDs at 350 nm (7.85×10^{-5}).[59] From the combined NMR data we estimate that the stoichiometry of the ligand shell to be for green QD-3, TOP = 4%, HPA = 78%, and HDA = 18%, and for yellow QD-3, TOP = 11%, HPA = 63%, and HDA = 26%. Combined with the molar concentration of QDs, this yields values for the total number of ligands per QD of ~230 and ~310 for green- and yellow-emitting QDs, respectively (see Table 1). These data are further combined with the nanocrystal size extracted from TEM measurements (see the Supporting Information) to extract an estimate for the ligand density per unit area, defined as the ratio between the total number of ligands and the QD surface area. The values reported in Table 1 clearly indicate that the measured densities for the green- and yellow-emitting QDs are comparable, which is consistent with the anticipated packed arrangement of the ligands on the nanocrystal surfaces.

Finally, we should note that ligand species and ligand coverage may vary depending on many factors involved in the growth reaction, such as coordinating solvent selection and added surfactants. The purification process also plays an important role when estimating the number of ligands in the organic cap, because ligand adsorption and desorption is a dynamic process, but the strength of the coordination interactions varies from one set of molecules to another. For instance, TOPO and TOP are important for the growth, but their coordination on the QD surface is weaker than those exhibited by phosphonate compounds.

3.4. DOSY Characterization of the QD Hydrodynamic Radius. TEM is a great characterization technique to measure the dimensions of various nanostructured materials, including those grown using solution phase techniques. However, because of its strong sensitivity to the electron density of the probed samples, it tends to only identify the dimensions of the inorganic components (usually made of transition metal atoms). For example, when applied to colloidal nanostructures, TEM characterization tends to miss the organic ligand shell.[1,58] For a variety of measurements such as tracking the diffusion of nanoparticles in biological media, the overall dimensions of the colloid (core-plus-organic shell) are often needed. This is referred to as the hydrodynamic size, and dynamic light scattering, DLS, has for a long time provided researchers with a powerful tool to extract such data for a variety of systems in solutions. These include polymeric colloidal spheres and inorganic nanocrystals.[65,66] However, DLS as a technique reaches its limit for very small nanocrystals, because the scattered signal becomes extremely weak (the scattered intensity varies as R^6, R being the size of the solute molecules). When applied to QDs, interference from the fluorescence emission of the nanocrystals themselves requires the use of only red laser sources (e.g., HeNe laser source with illumination at 632.8 nm). Also, only smaller QDs with emission below 633 nm can be accessed. Both requirements limit the effectiveness of this technique to probe QDs.[58,65,66] Fluorescence correlation spectroscopy can be used to extract such information, but it applies only to fluorescent nanocrystals, and requirements dealing with the nature of single molecule emission must be taken into account.[67,68]

DLS relies on the analysis of the normalized autocorrelation function of the scattered electric field, $g^{(1)}(\tau, q)$, as a function of the scattering wave vector ($q = \frac{4\pi n}{\lambda} \sin\left(\frac{\theta}{2}\right)$, with n being the refractive index of the medium), and decay time, τ.[65] For dispersions of colloidal nanoparticles (with small concentrations), $g^{(1)}(\tau, q)$ is commonly fit to a cumulants series:

$$g^{(1)}(\tau, q) = a \exp\left(-\Gamma\tau + \frac{\mu_2}{2}\tau^2 + \ldots\right) \quad (1)$$

where a is an experimental constant proportional to the amplitude of the scattered signal, while Γ and μ_2 designate the first and second cumulants, respectively. Γ corresponds to the decay rate expressed in terms of q and the diffusion coefficient, D ($\Gamma = Dq^2$), and the ratio μ_2/Γ^2 is the polydispersity index (PDI). To collect the DLS data we dispersed the purified QDs (only yellow-emitting dispersion) in toluene.

DOSY as a technique circumvents those issues as it probes the relaxation of the particular atomic shift with time (e.g., the shifts of various ^{1}H NMR protons in a molecule). The diffusion-weighted ^{1}H spectra can be measured by selectively filtering out the fast-diffusing species with a magnetic field gradient.[69,70] The signal attenuation is given by the Stejskal–Tanner equation:[71]

$$I = I_0 \exp\left(-(\gamma S_1 \delta G)^2 D\left(\Delta - S_2\delta - \frac{\tau}{2}\right)\right) \quad (2)$$

DOI: 10.1021/acs.chemmater.7b04204
Chem. Mater. 2018, 30, 225−238

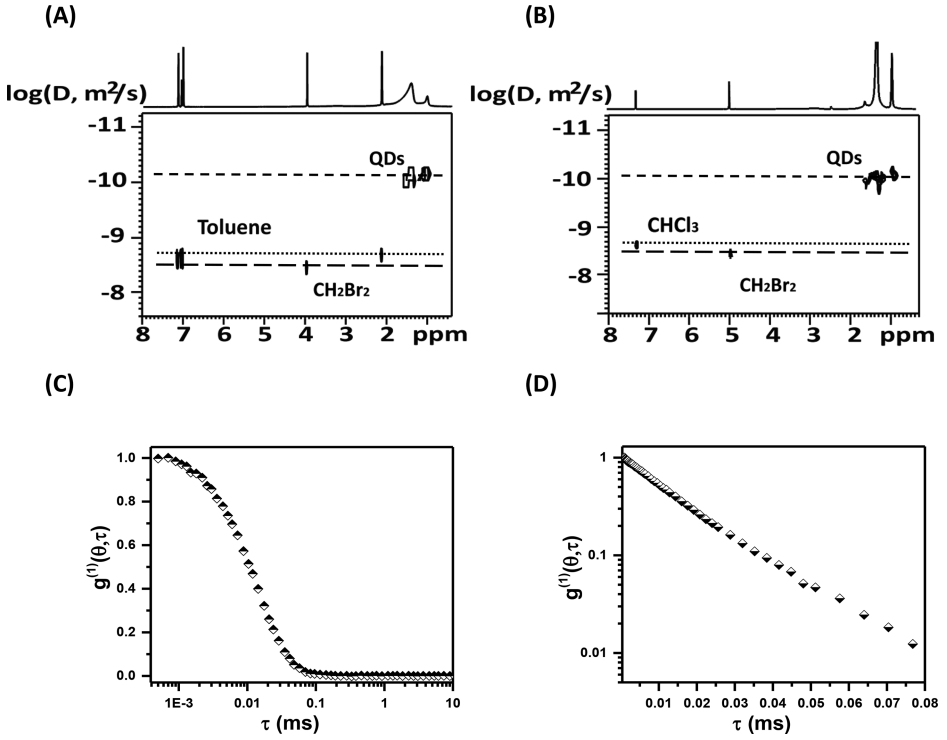

Figure 7. (A) DOSY of yellow-emitting QDs dispersed in toluene-d_8, QD-3 (after three rounds of purification). The hydrodynamic radius of the dots extracted from the diffusion coefficient is 4.0 nm. (B) DOSY of yellow-emitting QDs dispersed in chloroform-*d*, QD-3. The hydrodynamic radius of the dots extracted from the diffusion coefficient is 3.9 nm. (C, D) Representative plots of the electric field autocorrelation function $g^{(1)}(\theta, \tau)$ vs $\log(\tau)$ and $\log(g^{(1)}(\theta, \tau))$ vs τ, respectively. The hydrodynamic radius of the QDs extracted from dynamic light scattering measurement is $R_H \cong$ 4.1 nm.

Table 2. Values[a] for the Translational Diffusion Coefficient, *D*, and the Hydrodynamic Radius, R_H, Extracted from DOSY and DLS Measurements

sample	D_{DOSY}	D_{DLS}	η (mPa s)	$R_{H/DOSY}$	$R_{H/DLS}$
green QDs	1.05×10^{-10} m²/s	9.91×10^{-11} m²/s	0.5866, T = 293.5 K	3.5 nm	3.7 nm
yellow QDs	9.16×10^{-11} m²/s	8.94×10^{-11} m²/s	0.5866, T = 293.5 K	4.0 nm	4.1 nm

[a]Data were collected at room temperature (~293.5 K). The viscosity of toluene = 0.5886 cP (mPa s).

where γ is the proton gyromagnetic ratio, S_1 and S_2 are shape factors (correcting for the sinusoidal shape of the gradient pulse), G is the strength of gradient pulse, τ is the time interval between two bipolar gradient pulses, Δ is the diffusion time, δ is the gradient length and D is the diffusion coefficient.

The DOSY spectra were collected using QDs dispersed in toluene-d_8, an acquisition time = 2.0 s, a gradient strength G varying from 2% to 85% of the maximum gradient (45 G/cm), a diffusion delay time = 300 ms, a gradient pulse duration = 1.8 ms, and a relaxation delay = 5.0 s. Typical DOSY spectra collected from two sets of QDs (emitting at 540 and 570 nm), which have been subjected to two rounds of purification, are shown in Figures 4G and 7A, respectively. D is extracted from fitting the DOSY data to eq 2.

Generally, the diffusion coefficient, D, extracted from either DLS or DOSY is related to the hydrodynamic radius of the dispersed species by the well-known Stokes−Einstein equation:[66]

$$D = \frac{k_B T}{f_T} = \frac{k_B T}{6\pi\eta R_H} \tag{3}$$

where k_B is the Boltzmann constant (1.38×10^{-23} J/K), T is the temperature reported in Kelvin, f_T is the drag coefficient, and η is the viscosity of the solvent. The above equation indicates that the data on the diffusion coefficient can be further exploited to extract values for the hydrodynamic radius (R_H) of the dispersed nanocrystals. Table 2 summarizes side-by-side the measured values for D and R_H collected from DLS and DOSY techniques. There is clearly a good agreement between the values extracted from both measurements, which confirms that DOSY is an effective technique for extracting information about the diffusion coefficient and the hydrodynamic radius of colloidal QDs in solution phase. There is an additional clear advantage of DOSY, nonetheless. While DLS fails to yield accurate data for smaller sizes (1−3 nm), because of the rather small scattering signal in this size regime, DOSY, being strictly dependent on the proton shift, can yield accurate information on the diffusion coefficient of even solvent molecules as shown in Figures 4G and 7A. We do not aim to provide a thorough evaluation of the advantages and disadvantages of both techniques. That is beyond the scope of the present study, but may be further explored in future works.

4. CONCLUSION

We have exploited the noninvasiveness of solution NMR spectroscopy to characterize the structure and composition of

DOI: 10.1021/acs.chemmater.7b04204
Chem. Mater. 2018, 30, 225−238

the organic capping shell identified on the surfaces of CdSe−ZnS quantum dots grown using high-temperature reaction. Employing a combination of ^{31}P, ^{1}H, HSQC, and DOSY NMR supplemented by mass spectroscopy we have found that the nature and stoichiometry of the organic shell depend on the level of purification applied to the QD dispersion. In particular, our results show that as prepared the surface coating of CdSe−ZnS QDs is constituted of alkylamine, phosphorus molecules (e.g., TOP and TOPO), along with other phosphonic acid surfactants such as HPA. Coordination affinity of TOP and TOPO is weak, resulting in easy detachment of these ligands from the QD surface during purification, leaving only a small fraction of zinc- and sulfur-complexed TOPO and TOP molecules (as TOPO−Zn and TOP−S). Conversely, larger fractions of surface-bound phosphonic acid (HPA) and to a lesser extent hexadecyl amine (HDA) are identified on QDs subjected to three rounds of purification. This indicates that phosphonic acid ligands exhibit the strongest affinity to the metal-rich surfaces of the nanocrystals, a result consistent with prior findings on the organic cap of core-only QDs.

By combining ^{31}P, ^{1}H, ^{13}C, and DOSY NMR results collected from CdSe−ZnS QDs subjected to varying rounds of purification with MALDI mass spectroscopy data, collected from supernatant solutions of displaced ligands, we have been able to develop a model structure for the ligand shell composition on the surface of the nanocrystals. We have also been able to demonstrate that the QD hydrodynamic radii estimated from the DOSY technique are in good agreement with those extracted from dynamic light scattering measurements.

We believe that these NMR spectroscopy techniques can be successfully applied to characterize the organic coating of an array of other nanomaterials dispersed in a variety of solvents, either as prepared in organic media, or after cap exchange and transfer to completely different solvents (e.g., ligand exchange with water-compatible ligands and transfer to buffer media). Furthermore, NMR investigation of these materials can yield valuable information about the interplay between the various surfactants often combined to optimize their growth and enhance the PL yield. They can also yield crucial information about the roles played by the ligands in the steric stabilization of the nanocrystals.

■ ASSOCIATED CONTENT

Supporting Information

The Supporting Information is available free of charge on the ACS Publications website at DOI: 10.1021/acs.chemmater.7b04204.

Additional characterization of the ligands and QDs using NMR, DOSY, and FTIR measurements (PDF)

■ AUTHOR INFORMATION

Corresponding Author

*E-mail: mattoussi@chem.fsu.edu.

ORCID

Birong Zeng: 0000-0003-1582-4929
Wentao Wang: 0000-0003-2273-4171
Hedi Mattoussi: 0000-0002-6511-9323

Present Addresses

[§]N.Z.: Illumina Corp., 5200 Illumina Way, San Diego, CA 92122, USA.

[∥]W.W. and X.J.: Ocean Nanotech, LLC, 7964 Arjons Drive, San Diego, CA 92126, USA.

Notes

The authors declare no competing financial interest.

■ ACKNOWLEDGMENTS

We thank FSU and the National Science Foundation (NSF-CHE, Grants 1058957 and 1508501) and Asahi-Kasei Corp. for financial support, and acknowledge the support of the National Natural Science Foundation of China (51573150). We also thank Jan-Philip Merkl and Fadi Aldeek for assistance and for the helpful discussions.

■ REFERENCES

(1) Murray, C. B.; Norris, D. J.; Bawendi, M. G. Synthesis and Characterization of Nearly Monodisperse CdE (E = S, Se, Te) Semiconductor Nanocrystallites. *J. Am. Chem. Soc.* **1993**, *115*, 8706−8715.

(2) Bruchez, M., Jr.; Moronne, M.; Gin, P.; Weiss, S.; Alivisatos, A. P. Semiconductor Nanocrystals as Fluorescent Biological Labels. *Science* **1998**, *281*, 2013−2016.

(3) Coe, S.; Woo, W. K.; Bawendi, M.; Bulovic, V. Electroluminescence from Single Monolayers of Nanocrystals in Molecular Organic Devices. *Nature* **2002**, *420*, 800−803.

(4) Larson, D. R.; Zipfel, W. R.; Williams, R. M.; Clark, S. W.; Bruchez, M. P.; Wise, F. W.; Webb, W. W. Water-Soluble Quantum Dots for Multiphoton Fluorescence Imaging in Vivo. *Science* **2003**, *300*, 1434−1436.

(5) Resch-Genger, U.; Grabolle, M.; Cavaliere-Jaricot, S.; Nitschke, R.; Nann, T. Quantum Dots Versus Organic Dyes as Fluorescent Labels. *Nat. Methods* **2008**, *5*, 763−775.

(6) Talapin, D. V.; Lee, J. S.; Kovalenko, M. V.; Shevchenko, E. V. Prospects of Colloidal Nanocrystals for Electronic and Optoelectronic Applications. *Chem. Rev.* **2010**, *110*, 389−458.

(7) Lan, X.; Masala, S.; Sargent, E. H. Charge-Extraction Strategies for Colloidal Quantum Dot Photovoltaics. *Nat. Mater.* **2014**, *13*, 233−240.

(8) Colvin, V. L.; Schlamp, M. C.; Alivisatos, A. P. Light-Emitting Diodes Made from Cadmium Selenide Nanocrystals and a Semiconducting Polymer. *Nature* **1994**, *370*, 354−357.

(9) Medintz, I.; Uyeda, H.; Goldman, E.; Mattoussi, H. Quantum Dot Bioconjugates for Imaging, Labelling and Sensing. *Nat. Mater.* **2005**, *4*, 435−446.

(10) Gur, I.; Fromer, N. A.; Geier, M. L.; Alivisatos, A. P. Air-Stable All-Inorganic Nanocrystal Solar Cells Processed from Solution. *Science* **2005**, *310*, 462−465.

(11) Mattoussi, H.; Palui, G.; Na, H. B. Luminescent Quantum Dots as Platforms for Probing in Vitro and in Vivo Biological Processes. *Adv. Drug Delivery Rev.* **2012**, *64*, 138−166.

(12) Shirasaki, Y.; Supran, G. J.; Bawendi, M. G.; Bulovic, V. Emergence of Colloidal Quantum-Dot Light-Emitting Technologies. *Nat. Photonics* **2013**, *7*, 13−23.

(13) Bae, W. K.; Park, Y.-S.; Lim, J.; Lee, D.; Padilha, L. A.; McDaniel, H.; Robel, I.; Lee, C.; Pietryga, J. M.; Klimov, V. I. Controlling the Influence of Auger Recombination on the Performance of Quantum-Dot Light-Emitting Diodes. *Nat. Commun.* **2013**, *4*, 2661.

(14) Bullen, C.; Mulvaney, P. The Effects of Chemisorption on the Luminescence of CdSe Quantum Dots. *Langmuir* **2006**, *22*, 3007−3013.

(15) Kilina, S.; Ivanov, S.; Tretiak, S. Effect of Surface Ligands on Optical and Electronic Spectra of Semiconductor Nanoclusters. *J. Am. Chem. Soc.* **2009**, *131*, 7717−7726.

(16) Munro, A. M.; Jen-La Plante, I.; Ng, M. S.; Ginger, D. S. Quantitative Study of the Effects of Surface Ligand Concentration on CdSe Nanocrystal Photoluminescence. *J. Phys. Chem. C* **2007**, *111*, 6220−6227.

DOI: 10.1021/acs.chemmater.7b04204
Chem. Mater. 2018, 30, 225−238

(17) Kalyuzhny, G.; Murray, R. W. Ligand Effects on Optical Properties of CdSe Nanocrystals. *J. Phys. Chem. B* **2005**, *109*, 7012−7021.
(18) Hammer, N. I.; Early, K. T.; Sill, K.; Odoi, M. Y.; Emrick, T.; Barnes, M. D. Coverage-Mediated Suppression of Blinking in Solid State Quantum Dot Conjugated Organic Composite Nanostructures. *J. Phys. Chem. B* **2006**, *110*, 14167−14171.
(19) Qu, L. H.; Peng, Z. A.; Peng, X. G. Alternative Routes toward High Quality CdSe Nanocrystals. *Nano Lett.* **2001**, *1*, 333−337.
(20) Peng, Z. A.; Peng, X. G. Formation of High-Quality CdTe, CdSe, and CdS Nanocrystals Using CdO as Precursor. *J. Am. Chem. Soc.* **2001**, *123*, 183−184.
(21) Bullen, C. R.; Mulvaney, P. Nucleation and Growth Kinetics of CdSe Nanocrystals in Octadecene. *Nano Lett.* **2004**, *4*, 2303−2307.
(22) Jasieniak, J.; Mulvaney, P. From Cd-Rich to Se-Rich − the Manipulation of CdSe Nanocrystal Surface Stoichiometry. *J. Am. Chem. Soc.* **2007**, *129*, 2841−2848.
(23) Schreuder, M. A.; McBride, J. R.; Dukes, A. D.; Sammons, J. A.; Rosenthal, S. J. Control of Surface State Emission Via Phosphonic Acid Modulation in Ultrasmall CdSe Nanocrystals: The Role of Ligand Electronegativity. *J. Phys. Chem. C* **2009**, *113*, 8169−8176.
(24) Kovalenko, M. V.; Scheele, M.; Talapin, D. V. Colloidal Nanocrystals with Molecular Metal Chalcogenide Surface Ligands. *Science* **2009**, *324*, 1417−1420.
(25) Brown, P. R.; Kim, D.; Lunt, R. R.; Zhao, N.; Bawendi, M. G.; Grossman, J. C.; Bulović, V. Energy Level Modification in Lead Sulfide Quantum Dot Thin Films through Ligand Exchange. *ACS Nano* **2014**, *8*, 5863−5872.
(26) Hines, D. A.; Kamat, P. V. Recent Advances in Quantum Dot Surface Chemistry. *ACS Appl. Mater. Interfaces* **2014**, *6*, 3041−3057.
(27) Hines, D. A.; Kamat, P. V. Quantum Dot Surface Chemistry: Ligand Effects and Electron Transfer Reactions. *J. Phys. Chem. C* **2013**, *117*, 14418−14426.
(28) Puzder, A.; Williamson, A. J.; Zaitseva, N.; Galli, G.; Manna, L.; Alivisatos, A. P. The Effect of Organic Ligand Binding on the Growth of CdSe Nanoparticles Probed by Ab Initio Calculations. *Nano Lett.* **2004**, *4*, 2361−2365.
(29) Buckley, J. J.; Couderc, E.; Greaney, M. J.; Munteanu, J.; Riche, C. T.; Bradforth, S. E.; Brutchey, R. L. Chalcogenol Ligand Toolbox for CdSe Nanocrystals and Their Influence on Exciton Relaxation Pathways. *ACS Nano* **2014**, *8*, 2512−2521.
(30) Nag, A.; Kovalenko, M. V.; Lee, J.-S.; Liu, W.; Spokoyny, B.; Talapin, D. V. Metal-Free Inorganic Ligands for Colloidal Nanocrystals: S^{2-}, HS^{-}, Se^{2-}, HSe^{-}, Te^{2-}, HTe^{-}, TeS_3^{2-}, OH^{-}, and NH_2^{-} as Surface Ligands. *J. Am. Chem. Soc.* **2011**, *133*, 10612−10620.
(31) Law, M.; Luther, J. M.; Song, Q.; Hughes, B. K.; Perkins, C. L.; Nozik, A. J. Structural, Optical, and Electrical Properties of PbSe Nanocrystal Solids Treated Thermally or with Simple Amines. *J. Am. Chem. Soc.* **2008**, *130*, 5974−5985.
(32) Katari, J. E. B.; Colvin, V. L.; Alivisatos, A. P. X-Ray Photoelectron Spectroscopy of CdSe Nanocrystals with Applications to Studies of the Nanocrystal Surface. *J. Phys. Chem.* **1994**, *98*, 4109−4117.
(33) Dabbousi, B. O.; RodriguezViejo, J.; Mikulec, F. V.; Heine, J. R.; Mattoussi, H.; Ober, R.; Jensen, K. F.; Bawendi, M. G. (CdSe)ZnS Core-Shell Quantum Dots: Synthesis and Characterization of a Size Series of Highly Luminescent Nanocrystallites. *J. Phys. Chem. B* **1997**, *101*, 9463−9475.
(34) Foster, A. J.; Lobo, R. F. Identifying Reaction Intermediates and Catalytic Active Sites through in Situ Characterization Techniques. *Chem. Soc. Rev.* **2010**, *39*, 4783−4793.
(35) Sachleben, J. R.; Colvin, V.; Emsley, L.; Wooten, E. W.; Alivisatos, A. P. Solution-State NMR Studies of the Surface Structure and Dynamics of Semiconductor Nanocrystals. *J. Phys. Chem. B* **1998**, *102*, 10117−10128.
(36) Ribot, F.; Escax, V.; Roiland, C.; Sanchez, C.; Martins, J. C.; Biesemans, M.; Verbruggen, I.; Willem, R. In Situ Evaluation of Interfacial Affinity in CeO_2 Based Hybrid Nanoparticles by Pulsed Field Gradient NMR. *Chem. Commun.* **2005**, 1019−1021.
(37) Moreels, I.; Fritzinger, B.; Martins, J. C.; Hens, Z. Surface Chemistry of Colloidal PbSe Nanocrystals. *J. Am. Chem. Soc.* **2008**, *130*, 15081−15086.
(38) Virieux, H.; Le Troedec, M.; Cros-Gagneux, A.; Ojo, W.-S.; Delpech, F.; Nayral, C.; Martinez, H.; Chaudret, B. InP/ZnS Nanocrystals: Coupling NMR and XPS for Fine Surface and Interface Description. *J. Am. Chem. Soc.* **2012**, *134*, 19701−19708.
(39) Cros-Gagneux, A.; Delpech, F.; Nayral, C.; Cornejo, A.; Coppel, Y.; Chaudret, B. Surface Chemistry of InP Quantum Dots: A Comprehensive Study. *J. Am. Chem. Soc.* **2010**, *132*, 18147−18157.
(40) Morris-Cohen, A. J.; Malicki, M.; Peterson, M. D.; Slavin, J. W. J.; Weiss, E. A. Chemical, Structural, and Quantitative Analysis of the Ligand Shells of Colloidal Quantum Dots. *Chem. Mater.* **2013**, *25*, 1155−1165.
(41) Knittel, F.; Gravel, E.; Cassette, E.; Pons, T.; Pillon, F.; Dubertret, B.; Doris, E. On the Characterization of the Surface Chemistry of Quantum Dots. *Nano Lett.* **2013**, *13*, 5075−5078.
(42) Shen, Y.; Gee, M. Y.; Tan, R.; Pellechia, P. J.; Greytak, A. B. Purification of Quantum Dots by Gel Permeation Chromatography and the Effect of Excess Ligands on Shell Growth and Ligand Exchange. *Chem. Mater.* **2013**, *25*, 2838−2848.
(43) Morris-Cohen, A. J.; Donakowski, M. D.; Knowles, K. E.; Weiss, E. A. The Effect of a Common Purification Procedure on the Chemical Composition of the Surfaces of CdSe Quantum Dots Synthesized with Trioctylphosphine Oxide. *J. Phys. Chem. C* **2010**, *114*, 897−906.
(44) Donakowski, M. D.; Godbe, J. M.; Sknepnek, R.; Knowles, K. E.; Olvera de la Cruz, M.; Weiss, E. A. A Quantitative Description of the Binding Equilibria of Para-Substituted Aniline Ligands and CdSe Quantum Dots. *J. Phys. Chem. C* **2010**, *114*, 22526−22534.
(45) Anderson, N. C.; Owen, J. S. Soluble, Chloride-Terminated CdSe Nanocrystals: Ligand Exchange Monitored by ^{1}H and ^{31}P NMR Spectroscopy. *Chem. Mater.* **2013**, *25*, 69−76.
(46) Owen, J.; Brus, L. Chemical Synthesis and Luminescence Applications of Colloidal Semiconductor Quantum Dots. *J. Am. Chem. Soc.* **2017**, *139*, 10939−10943.
(47) Wang, F.; Tang, R.; Buhro, W. E. The Trouble with TOPO; Identification of Adventitious Impurities Beneficial to the Growth of Cadmium Selenide Quantum Dots, Rods, and Wires. *Nano Lett.* **2008**, *8*, 3521−3524.
(48) Wang, F.; Tang, R.; Kao, J. L. F.; Dingman, S. D.; Buhro, W. E. Spectroscopic Identification of Tri-N-Octylphosphine Oxide (TOPO) Impurities and Elucidation of Their Roles in Cadmium Selenide Quantum-Wire Growth. *J. Am. Chem. Soc.* **2009**, *131*, 4983−4994.
(49) Hassinen, A.; Gomes, R.; De Nolf, K.; Zhao, Q.; Vantomme, A.; Martins, J. C.; Hens, Z. Surface Chemistry of CdTe Quantum Dots Synthesized in Mixtures of Phosphonic Acids and Amines: Formation of a Mixed Ligand Shell. *J. Phys. Chem. C* **2013**, *117*, 13936−13943.
(50) De Nolf, K.; Cosseddu, S. M.; Jasieniak, J. J.; Drijvers, E.; Martins, J. C.; Infante, I.; Hens, Z. Binding and Packing in Two-Component Colloidal Quantum Dot Ligand Shells: Linear Versus Branched Carboxylates. *J. Am. Chem. Soc.* **2017**, *139*, 3456−3464.
(51) Gomes, R.; Hassinen, A.; Szczygiel, A.; Zhao, Q.; Vantomme, A.; Martins, J. C.; Hens, Z. Binding of Phosphonic Acids to CdSe Quantum Dots: A Solution NMR Study. *J. Phys. Chem. Lett.* **2011**, *2*, 145−152.
(52) Hens, Z.; Martins, J. C. A Solution NMR Toolbox for Characterizing the Surface Chemistry of Colloidal Nanocrystals. *Chem. Mater.* **2013**, *25*, 1211−1221.
(53) Anderson, N. C.; Hendricks, M. P.; Choi, J. J.; Owen, J. S. Ligand Exchange and the Stoichiometry of Metal Chalcogenide Nanocrystals: Spectroscopic Observation of Facile Metal-Carboxylate Displacement and Binding. *J. Am. Chem. Soc.* **2013**, *135*, 18536−18548.
(54) Qu, L.; Peng, X. Control of Photoluminescence Properties of CdSe Nanocrystals in Growth. *J. Am. Chem. Soc.* **2002**, *124*, 2049−2055.
(55) Davidowski, S. K.; Lisowski, C. E.; Yarger, J. L. Characterizing Mixed Phosphonic Acid Ligand Capping on CdSe/ZnS Quantum

DOI: 10.1021/acs.chemmater.7b04204
Chem. Mater. 2018, 30, 225−238

Dots Using Ligand Exchange and NMR Spectroscopy. *Magn. Reson. Chem.* **2016**, *54*, 234−238.
(56) Clapp, A. R.; Goldman, E. R.; Mattoussi, H. Capping of CdSe-ZnS Quantum Dots with DHLA and Subsequent Conjugation with Proteins. *Nat. Protoc.* **2006**, *1*, 1258−1266.
(57) Hines, M. A.; Guyot-Sionnest, P. Synthesis and Characterization of Strongly Luminescing ZnS-Capped CdSe Nanocrystals. *J. Phys. Chem.* **1996**, *100*, 468−471.
(58) Mattoussi, H.; Cumming, A. W.; Murray, C. B.; Bawendi, M. G.; Ober, R. Properties of CdSe Nanocrystal Dispersions in the Dilute Regime: Structure and Interparticle Interactions. *Phys. Rev. B: Condens. Matter Mater. Phys.* **1998**, *58*, 7850−7863.
(59) Leatherdale, C. A.; Woo, W. K.; Mikulec, F. V.; Bawendi, M. G. On the Absorption Cross Section of CdSe Nanocrystal Quantum Dots. *J. Phys. Chem. B* **2002**, *106*, 7619−7622.
(60) Peterson, M. D.; Cass, L. C.; Harris, R. D.; Edme, K.; Sung, K.; Weiss, E. A. The Role of Ligands in Determining the Exciton Relaxation Dynamics in Semiconductor Quantum Dots. *Annu. Rev. Phys. Chem.* **2014**, *65*, 317−339.
(61) Giovanelli, E.; Muro, E.; Sitbon, G.; Hanafi, M.; Pons, T.; Dubertret, B.; Lequeux, N. Highly Enhanced Affinity of Multidentate Versus Bidentate Zwitterionic Ligands for Long-Term Quantum Dot Bioimaging. *Langmuir* **2012**, *28*, 15177−15184.
(62) Wehrli, F. W.; Wirthlin, T. *Interpretation of Carbon-13 NMR Spectra*; Heyden, 1976.
(63) Chen, P. E.; Anderson, N. C.; Norman, Z. M.; Owen, J. S. Tight Binding of Carboxylate, Phosphonate, and Carbamate Anions to Stoichiometric CdSe Nanocrystals. *J. Am. Chem. Soc.* **2017**, *139*, 3227−3236.
(64) Son, J. G.; Choi, E.; Piao, Y.; Han, S. W.; Lee, T. G. Probing Organic Ligands and Their Binding Schemes on Nanocrystals by Mass Spectrometric and FT-IR Spectroscopic Imaging. *Nanoscale* **2016**, *8*, 4573−4578.
(65) Pons, T.; Uyeda, H. T.; Medintz, I. L.; Mattoussi, H. Hydrodynamic Dimensions, Electrophoretic Mobility, and Stability of Hydrophilic Quantum Dots. *J. Phys. Chem. B* **2006**, *110*, 20308−20316.
(66) Berne, B. J.; Pecora, R. *Dynamic Light Scattering: With Applications to Chemistry, Biology, and Physics*, Dover Ed.; Dover Publications: Mineola, NY, 2000; pp vii, 376.
(67) Doose, S.; Tsay, J. M.; Pinaud, F.; Weiss, S. Comparison of Photophysical and Colloidal Properties of Biocompatible Semiconductor Nanocrystals Using Fluorescence Correlation Spectroscopy. *Anal. Chem.* **2005**, *77*, 2235−2242.
(68) Liedl, T.; Keller, S.; Simmel, F. C.; Rädler, J. O.; Parak, W. J. Fluorescent Nanocrystals as Colloidal Probes in Complex Fluids Measured by Fluorescence Correlation Spectroscopy. *Small* **2005**, *1*, 997−1003.
(69) Morris, K. F.; Johnson, C. S. Diffusion-Ordered Two-Dimensional Nuclear Magnetic Resonance Spectroscopy. *J. Am. Chem. Soc.* **1992**, *114*, 3139−3141.
(70) Novoa-Carballal, R.; Fernandez-Megia, E.; Jimenez, C.; Riguera, R. NMR Methods for Unravelling the Spectra of Complex Mixtures. *Nat. Prod. Rep.* **2011**, *28*, 78−98.
(71) Stejskal, E. O.; Tanner, J. E. Spin Diffusion Measurements: Spin Echoes in the Presence of a Time-Dependent Field Gradient. *J. Chem. Phys.* **1965**, *42*, 288−292.
(72) Green, M. L. H.; Parkin, G. Application of the Covalent Bond Classification Method for the Teaching of Inorganic Chemistry. *J. Chem. Educ.* **2014**, *91*, 807−816.

DOI: 10.1021/acs.chemmater.7b04204
Chem. Mater. 2018, 30, 225−238